Identification of Potent ADCK3 Inhibitors through Structure-Based Virtual Screening

Peng Gao, Mitali Tambe, Catherine Z. Chen, Wenwei Huang, Gregory J. Tawa, Tal Hirschhorn, Brent R. Stockwell, Wei Zheng,* and Min Shen*

ABSTRACT: ADCK3 is a member of the UbiB family of atypical protein kinases in humans, with homologues in archaea, bacteria, and eukaryotes. In lieu of protein kinase activity, ADCK3 plays a role in the biosynthesis of coenzyme Q10 (CoQ10), and inactivating mutations can cause a CoQ10 deficiency and ataxia. However, the exact functions of ADCK3 are still unclear, and small-molecule inhibitors could be useful as chemical probes to elucidate its molecular mechanisms. In this study, we applied structure-based virtual screening (VS) to discover a novel chemical series of ADCK3 inhibitors. Through extensive structural analysis of the active-site residues, we developed a pharmacophore model and applied it to a large-scale VS. Out of ~170,000 compounds virtually screened, 800 top-ranking candidate compounds were selected and tested in both ADCK3 and p38 biochemical assays for hit validation. In total, 129 compounds were confirmed as ADCK3 inhibitors, and among them, 114 compounds are selective against p38, which was used as a counter-target. Molecular dynamics (MD) simulations were then conducted to predict the binding modes of the most potent compounds within the ADCK3 active site. Through metadynamics analysis, we successfully detected the key amino acid residues that govern intermolecular interactions. The findings provided in this study can serve as a promising starting point for drug development.
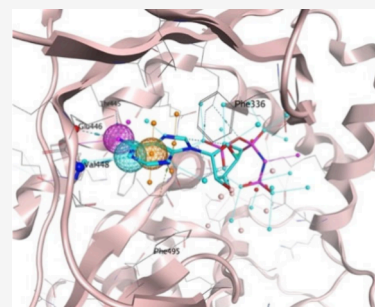
INTRODUCTION

The UbiB kinase-like proteins are an ancient family of atypical protein kinases with homologues in archaea, bacteria, and eukaryotes. In eukaryotes, the UbiB homologues reside exclusively in the mitochondria and function in coenzyme Q10 (CoQ10) biosynthesis.[1] CoQ10 is a lipophilic molecule ubiquitously present in all cell membranes and functions as an enzyme cofactor in the transfer of electrons in the respiratory chain.[2] Mutations in a human UbiB homologue, ADCK3 (COQ8A), cause a primary CoQ10 deficiency leading to neurodegeneration and ataxia.[3] ADCK3 does not have detectable protein kinase activity; instead, its ATPase activity is necessary for its role in CoQ10 biosynthesis and in stabilizing the CoQ biosynthetic complex.[4] However, the exact mechanism by which ADCK3 functions is unclear, and small-molecule inhibitors could be used as molecular tools to help probe the molecular functions of ADCK3.

Currently, no selective ADCK3 inhibitors have been reported, although crystallographic studies have revealed unique features of ADCK3 that could be targeted. Stefely et al. described the substrate binding pocket in a solved X-ray structure at a resolution of 2.3 Å, in complex with adenosine 5′-(β,γ-imido)triphosphate (AMPPNP).[4] This structure provided molecular insight into the binding pocket and demonstrated that ADCK3 adopts an atypical protein kinase-like fold. These results suggest a model wherein the inhibition of protein kinase

activity is important for the mechanism by which ADCK3 can enable CoQ10 biosynthesis.

In order to identify potent ADCK3 inhibitors, we developed a robust virtual screening strategy, screened large and diverse chemical libraries, and evaluated the activity of candidate compounds in biochemical assays. Before large-scale docking calculations were carried out to score millions of candidate compounds, a pharmacophore model of the ADCK3 active site was first generated and characterized quantitatively to guide the virtual screening. The general workflow of the combinational screening strategy is described in Figure 1. In total, ~170,000 compounds were first screened by molecular docking. The top ranking virtual screening hits were tested in our biochemical assays (ADCK3 and p38) in dose response to evaluate their biological activity and selectivity, and the most potent compounds were further selected for molecular dynamics (MD) simulations to investigate their possible binding modes with the target protein.[5] A total of 129 compounds showed inhibitory activity in the ADCK3 biochemical assay, and among them, 114 compounds show
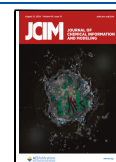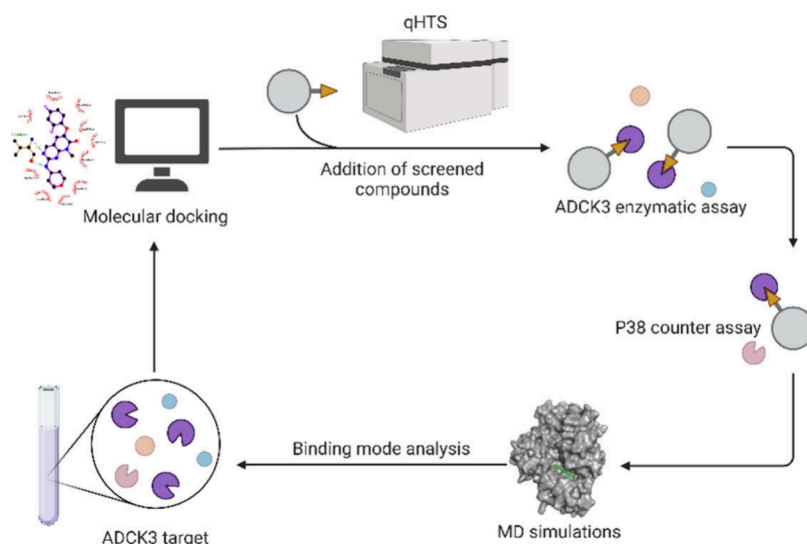
Figure 1. Workflow of drug screening using biochemical assays and structure-based modeling.

selectivity against the counter-target p38. The ADCK3 inhibitors identified from this virtual screening not only can be used to probe ADCK3 functions in disease models but also serve as supportive feedback for assay development and optimization, including cell-based ADCK3 assays for future screens. Additionally, the computational approach described herein could provide a robust virtual screening strategy for lead identification in early stage drug development.

EXPERIMENTAL SECTION

Protein Structure Preparation and Pharmacophore Modeling. The three-dimensional (3D) structure of ADCK3 was downloaded from the Protein Data Bank (PDB code 5I35). The structure is complexed with phosphoaminophosphonic acid-adenylate ester (AMPPNP), an ATP mimetic, within the active site. Preparation work, including removing nonstructural water molecules, hydrogen addition, protonation, and conformational optimization, was performed using Mgtools 1.5.6. The pharmacophore model was generated using the MOE program.[6] The cocrystallized AMPPNP bound at the active site of ADCK3 was used as a pharmacophore query. The key pharmacophore features contain two hydrogen-bond (HB) donors, one HB acceptor, one hydrophobic interaction center, and one electrostatic interaction center (Figure 2). The pharmacophore model was used as a constraint in docking-based virtual screening.

NCATS Libraries for Virtual Screening. The Sytravon library is an in-house collection containing ∼44,000 small molecules with chemically diverse and novel structures, and most of them have medicinal chemistry-tractable scaffolds. The Genesis library containing ∼110,000 compounds was assembled to provide a novel modern chemical library that emphasizes high-quality chemical starting points, sp^3-enriched chemotypes, and core scaffolds that enable rapid purchase and derivatization via medicinal chemistry. The NCATS Pharmacologically Active Chemical Toolbox (NPACT) is a collection of ∼5,000 annotated biologically active compounds. In total, more than 7,000 mechanisms and phenotypes have been indicated in patents and the published literature, with a wide coverage of biological interactions in microbial, mammalian, plant, and other related systems. The evaluations of the physicochemical properties of these three libraries as well as
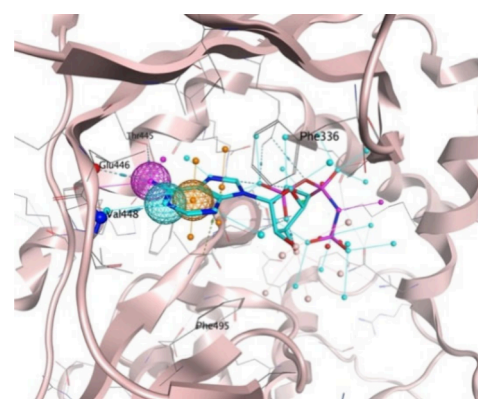

Figure 2. Predicted pharmacophore model is based on the ADCK3 cocrystal structure. The purple, cyan, and orange spheres represent H-bond donors, H-bond acceptors, and aromatic rings, respectively. All possible pharmacophoric elements within the active site are shown with little annotation points.

their structural diversity coverage can be found in our previous study.[7]

Molecular Docking. The AutoDock Vina 1.1.2 program[8] was used for large-scale docking in order to identify potent inhibitors for ADCK3 against ∼170,000 compounds from the three libraries mentioned above. None of them had been experimentally tested in ADCK3 or p38 enzyme assays. The default parameters in AutoDock Vina 1.1.2 were set up with AutoDockTools.[9] The affinity values obtained from docking indicate the strength of the binding interaction between the ADCK3 active site and the candidate compounds. The top-ranked candidate compounds were retained for visual inspection and postprocessing.[10] The consensus hits with the lowest binding free energies and reasonable docking orientations were selected for experimental evaluation.

Molecular Dynamics (MD) Simulation and Metadynamics Analysis. MD simulations were performed at a temperature of 310 K to describe the binding interaction between the target protein ADCK3 and the identified inhibitors. All of the calculations were conducted with GROMACS 2019.6. The CHARMM 27 force field[11] was adopted, and the virtual screening hits were processed with the
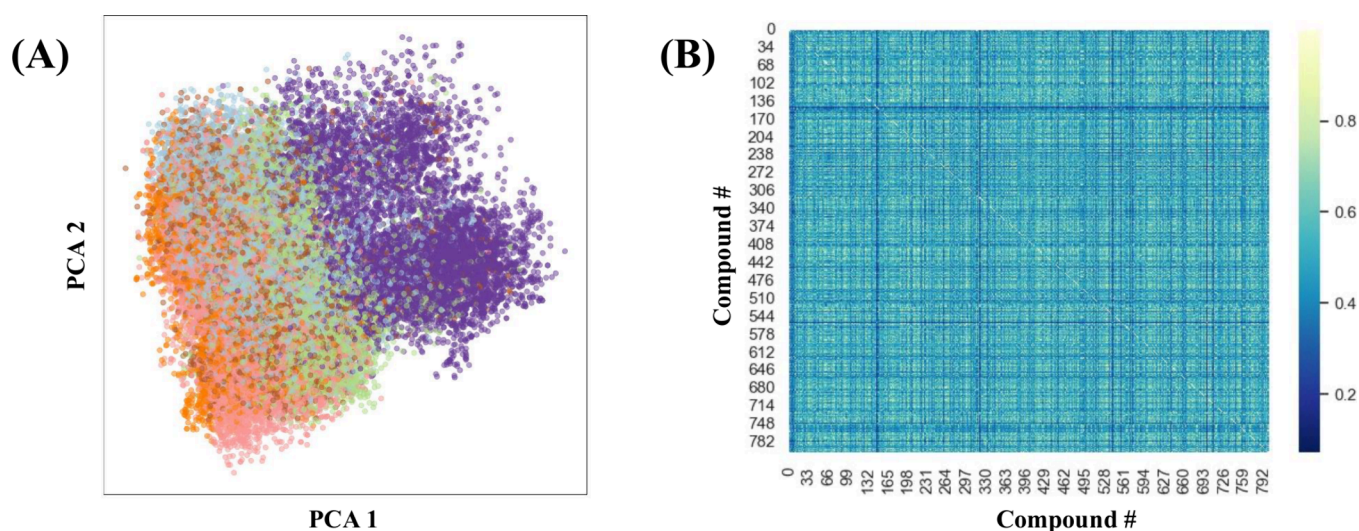
Figure 3. (A). The clustering of the screened molecules by PCA. Each color within the visual representation corresponds to an individual cluster. (B) The similarity matrix of the top 800 virtual screening hits.

NVT ensemble.[12] The size of the unit cell was defined as $80 \times 80 \times 80$ Å^3 to fully encompass the entire ADCK3 protein. The SPC/E model was employed to simulate water molecules,[13] and the concentration of the applied NaCl was 0.9%. The total simulation time was 200 ns, and the time step was set to 2 fs. For each simulation, three replica copies starting from different coordinates and velocities were used. The V-rescale approach was employed for temperature coupling,[14] and the Berendsen method[15] was used for pressure coupling. Energy minimization prior to MD simulations was performed using the steepest descent method within the first 5,000 steps, and after 20 ns of NVT simulations, NPT simulations were conducted. The calculated binding free energies for these compounds were presented for reference for experimental work. The binding free energies (in kcal/mol) were calculated by the g_mmpbsa package, with the MM/PBSA method applied. To systematically explore the binding modes of the identified compounds, we utilized metadynamics analysis to facilitate enhanced sampling for global minimal conformation searching. Principal components were calculated by using superposed α-carbon coordinates throughout the trajectories. Conformational free energy changes were mapped as a function of the root-mean-square deviation (RMSD) and radius of gyration measurements across each trajectory. GROMACS sham software was employed to generate the free energy landscapes.

ADCK3 Biochemical Assay. Components from a commercially available LanthaScreen time-resolved fluorescent resonance energy transfer (TR-FRET)-based assay for ADCK3 (Life Technologies; Carlsbad, CA, USA) were used for this study. For the assay, all of the reagent solutions were prepared using Kinase buffer A (Thermo Fisher Scientific, catalog no. PV3189). The assay was performed in a white 1536 well, solid bottom, medium binding assay plate (GNF ref no. 789175F). Briefly, 2 μL of recombinant GST-ADCK3 (Thermo Fisher, catalog no. A30969) was dispensed into each well at a final concentration of 5 nM using a Bioraptr2 FRD (Beckman Coulter, Brea, CA). Next, 23 nL of the compounds was pin transferred into the wells using an NX-TR pintool workstation (Wako Automation, San Diego, CA) and incubated with ADCK3 at room temperature for 15 min. Next, 1 μL of the competitive binding tracer (Kinase Tracer 178; catalog no.

PV5593) at final concentration of 100 nM and 1 μL of the europium-anti-GST antibody (catalog no. PV5593) at final concentration of 1 nM were dispensed into the wells using the Bioraptr dispenser. The reaction was allowed to proceed at room temperature for 30 min before the TR-FRET signal was measured on the Envision multimode plate reader (PerkinElmer, Shelton, CT) using the dual-emission HTRF module (665 nm/615 nm). SGC-GAK1, a previously published ADCK3 inhibitor,[16] was used as a positive control for this assay. The data was plotted as % ADCK3 inhibition, which was normalized as 0% inhibition being the DMSO control and −100% inhibition being 287.5 μM SGC-GAK1.

p38 Biochemical Assay. For the p38 assay, the same protocol was followed with components specific to p38. The specific components used were purified recombinant GST-MAPK14 (p38) protein (Thermo Fisher Scientific, catalog no. PV3304), final concentration 5 nM, and Kinase tracer 199 (Thermo Fisher Scientific, catalog no. PV5830), final concentration 100 nM. The data was normalized to % p38 inhibition, with 0% inhibition being the DMSO control and −100% inhibition being treatment with 287.5 μM SB202190, a known p38.[17]

■ RESULTS AND DISCUSSION

Pharmacophore-Based Virtual Screening Approach. We thoroughly examined the interaction landscape between the ATP mimetic AMPPNP within the active site based on the crystal structure 5I35, and we developed a pharmacophore model aimed at identifying novel ADCK3 inhibitors. As shown in Figure 2, three pharmacophore features representing the anchoring force were selected. As mentioned, one feature is an H-bond donor (purple sphere) that is located at the − NH$_2$ group of the adenine core interacting with the backbone carbonyl oxygen of Glu446. The second feature is an H-bond acceptor (cyan sphere) from the adenine ring nitrogen, forming an interaction with backbone −NH of Val448. Both features are key elements for protein kinase inhibitor design targeting the highly conserved hinge region. The third feature is an aromatic ring (orange sphere) that is located in the adenine core participating in a T-shaped π-stacking interaction with Phe336. It is worth mentioning that although extensive

hydrophilic interactions and H-bond potentials have been observed from the sugar and triphosphate moieties of AMPPNP with the neighboring residues, they are not considered to be crucial features as most protein kinase inhibitors do not mimic such interactions at the ATP binding site. Thus, only three key features from the adenine core were included in the pharmacophore model for constraint docking and virtual screening.

We carried out a virtual screen using this predefined three-point pharmacophore to search for novel inhibitors of ADCK3. Initially, we redocked the cocrystal ligand AMPPNP, an ATP mimetic, into the ACCK3 active site and derived the docking score as the threshold. After performing large-scale virtual screening against our in-house collection of ~170,000 compounds, we selected the top 800 candidate hits that passed this score threshold for experimental validation. The clustering analysis of this entire library using principal components analysis (PCA) is shown in Figure 3A, which indicates a diverse chemical space for virtual screening. To identify hits with diverse chemical scaffolds and features, we set up the query filters to be less stringent initially; i.e., any compounds that satisfy two out of three pharmacophore features will be selected by the molecular docking and scoring process. The pairwise similarity matrix of these identified hits is shown in Figure 3B, with a Tanimoto coefficient of ≤0.5 for most of the compounds, further demonstrating a considerable diversity coverage of the screening result.

Experimental Validation of Virtual Screening Hits. A biochemical ADCK3 assay was utilized to experimentally evaluate the 800 virtual screening hits. The assay was based on LanthaScreen time-resolved FRET (TR-FRET) technology to detect the ability of small-molecule compounds to displace a kinase tracer from the active site of recombinant GST-ADCK3 (Figure 4A). Out of the 800 compounds tested in the ADCK3 biochemical assay, 129 exhibited inhibitory activity (curve classes 1−3[18] and maximal response ≥30%), which corresponded to a virtual screening hit confirmation rate of 16.1%. We further tested these compounds in the p38 biochemical assay as a counter screen, and 114 compounds were confirmed to be potent and selective ADCK3 inhibitors. The best representative example hits are listed in Table 1, and the experimental validation data can be found in the Supporting Information. Remarkably, several compounds had potency in the nanomolar to single-digit micromolar range with full inhibition.

Since the virtual screening was conducted solely based on the ADCK3 structure, it was expected that some of the screening hits may also have activities in other protein kinases such as p38. As shown in Figure 4, NCGC00122705, NCGC00116016, NCGC00119692, and NCGC00117632 are potent inhibitors of ADCK3, with IC_{50} values ranging from 0.97 to 9.68 μM, with no inhibition of p38 at concentrations of up to 30 μM. Although NCGC00440171 showed inhibitory activity in both assays, the selectivity window is more than 10-fold against the p38 counter-target. Interestingly, NCGC00262195, the most potent ADCK3 inhibitor with an IC_{50} of 0.34 μM, also strongly inhibits p38 with IC_{50} of 0.017 μM. Furthermore, we examined NCGC00262195 and found that it has a reported kinase selectivity profile obtained through the KINOMEscan kinase screening.[19] It showed submicromolar inhibition for only 10 out of >300 kinases tested, suggesting a general clean profile and potential to explore substituents for optimal potency and
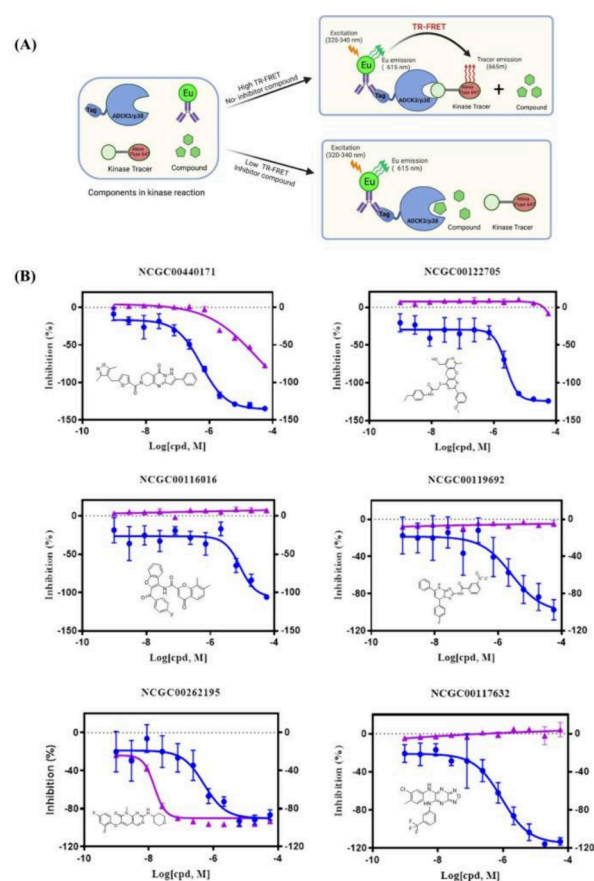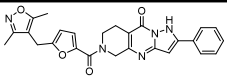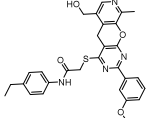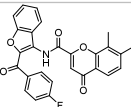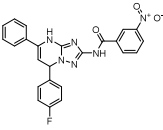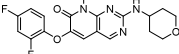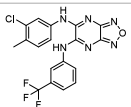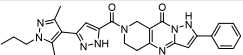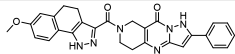

Figure 4. (A) Schematic of the biochemical assays. (B) Concentration−response curves of the top inhibitors in the ADCK3 (blue) and p38 (purple) biochemical assays. All concentration−response curves were derived from $n = 3$ biological replicate data, with the error bar showing standard deviation.

selectivity. These potent ADCK3 inhibitors directly identified from virtual screening could serve as tool molecules to study the underlying biology and were a good starting point for medicinal chemistry optimization.

We also noticed that some of the top-ranking hits are structurally similar. For example, NCGC00440171, NCGC00440319, and NCGC00440303 all share a tricyclic core. This inherent similarity within the in-house librarie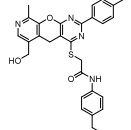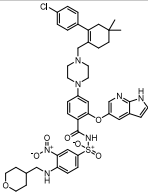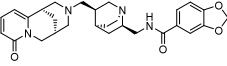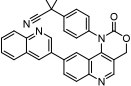s can lead to the identification of structurally similar hits, especially if certain scaffold types are well-represented. The pharmacophore features used in our initial screening were designed to capture essential interactions with the target. If specific chemical scaffolds naturally possess these critical features, then they may be preferentially selected, leading to similar hits. Compounds with similar scaffolds can offer insights into structure−activity relationships (SAR) and help refine the pharmacophore model for future screenings. Additionally, slight variations in similar compounds can significantly impact their biological activity, providing opportunities for optimization.

Docking Model of the Top-Ranking Virtual Screening Hits. To better understand the binding orientation and specific interactions, we examined the docking models for the representative top-ranking hits. As shown in Figure 5, NCGC00440171 maintains the H-bond interaction with the hinge region perfectly, with the phenyl ring inserting into the hydrophobic back pocket and the other terminal floating in the

6075

Table 1. Top-Ranking Compounds by Virtual Screening and Biochemical Assay Validation[a]

Compounds	Structure	ADCK3 assay		p38 assay		Free-energy (kJ/mol)[1]
		IC$_{50}$ (μM)	Efficacy (%)	IC$_{50}$ (μM)	Efficacy (%)	
NCGC00440171		0.49	-140.26	6.85	-89.53	-134.73 ± 3.63
NCGC00122705		2.17	-119.82	NA	-16.93	-128.93 ± 3.17
NCGC00116016		9.68	-136.50	NA	NA	-136.81 ± 4.11
NCGC00119692		3.85	-123.74	NA	NA	-105.74 ± 2.59
NCGC00262195		0.34	-89.81	0.02	-70.70	-128.46 ± 3.12
NCGC00117632		0.97	-119.62	NA	NA	-138.46 ± 4.20
NCGC00440319		1.72	-100.22	17.21	-48.08	NA
NCGC00440303		2.73	-102.01	NA	-24.79	NA
NCGC00122428		8.63	-141.53	NA	NA	NA
NCGC00345789		6.11	-138.53	NA	NA	NA
NCGC00399862		13.67	-128.74	NA	NA	NA
NCGC00386292		15.34	-95.33	30.61	-53.38	NA

[a]The free energy was calculated via MD simulation results.

solvent-exposed area. The central aromatic core also has a π−π interaction with Phe336 on top of the pocket.

NCGC00122705 could form only one H-bond to hinge region residue Val448 from its pyridine nitrogen based on the
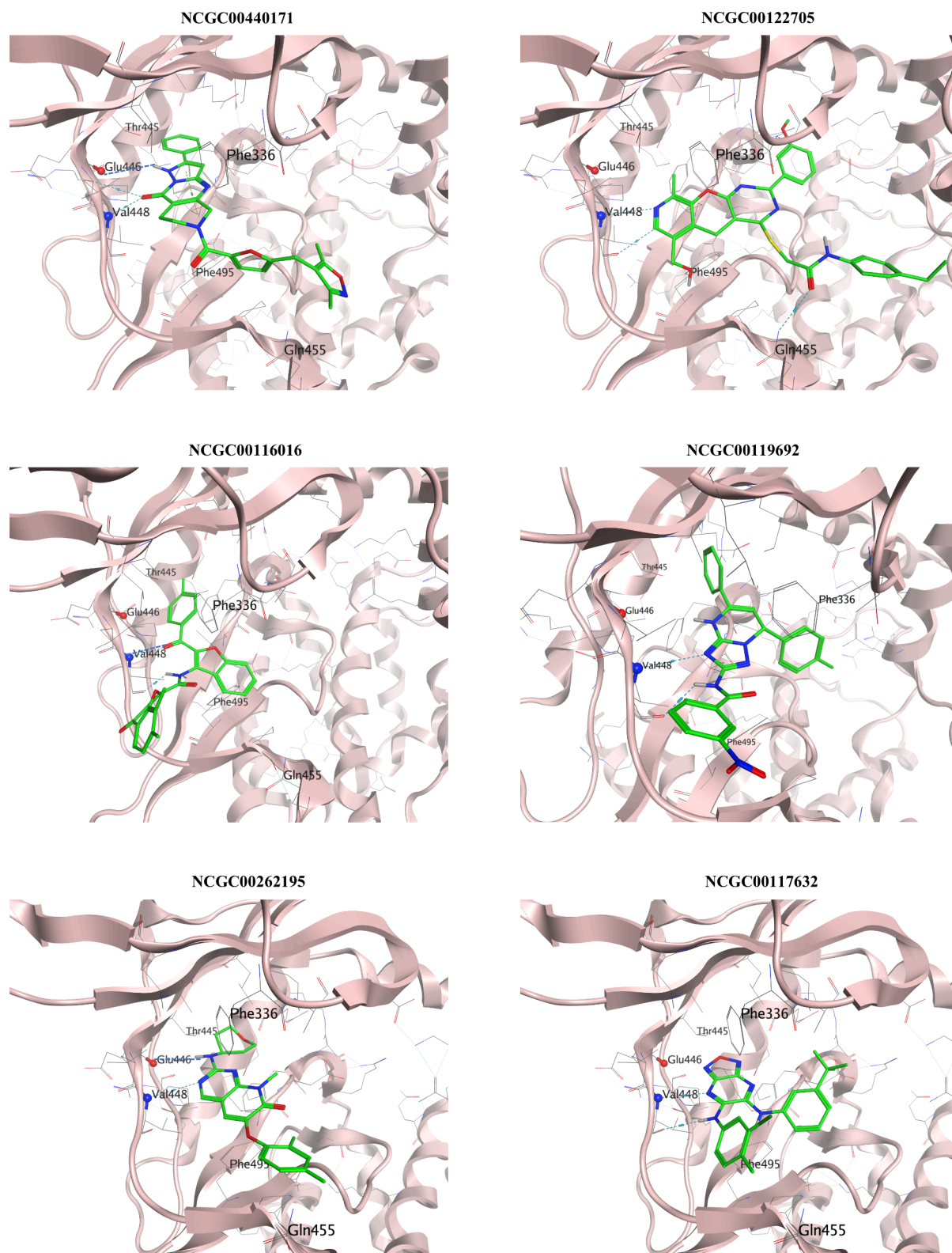
Figure 5. Predicted docking models for potent inhibitors within the ADCK3 active sites. The DFT-calculated molecular orbitals of these inhibitors can be found in Figure S1.

predefined pharmacophore, but the carbonyl oxygen of the amide linker also picks up another H-bond with Gln455. Similarly, NCGC00116016, NCGC00119692, and NCGC00117632 maintain only one of the key pharmacophore features in the hinge region to Val448, but the −NH linker in these three molecules also forms an additional H-bond to the

backbone carbonyl oxygen of Val448. This is the third H-bond interaction that could be potentially applied in kinase inhibitor design. NCGC00262195 forms two H-bonds which are mapped to the pharmacophore model, with tetrahydropyran positioned into the hydrophobic back pocket. In summary, both NCGC00440171 and NCGC00262195 could maintain

Figure 6. MD simulation results of the six screened compounds within the ADCK3 protein. Metadynamics analysis technology that utilizes the projections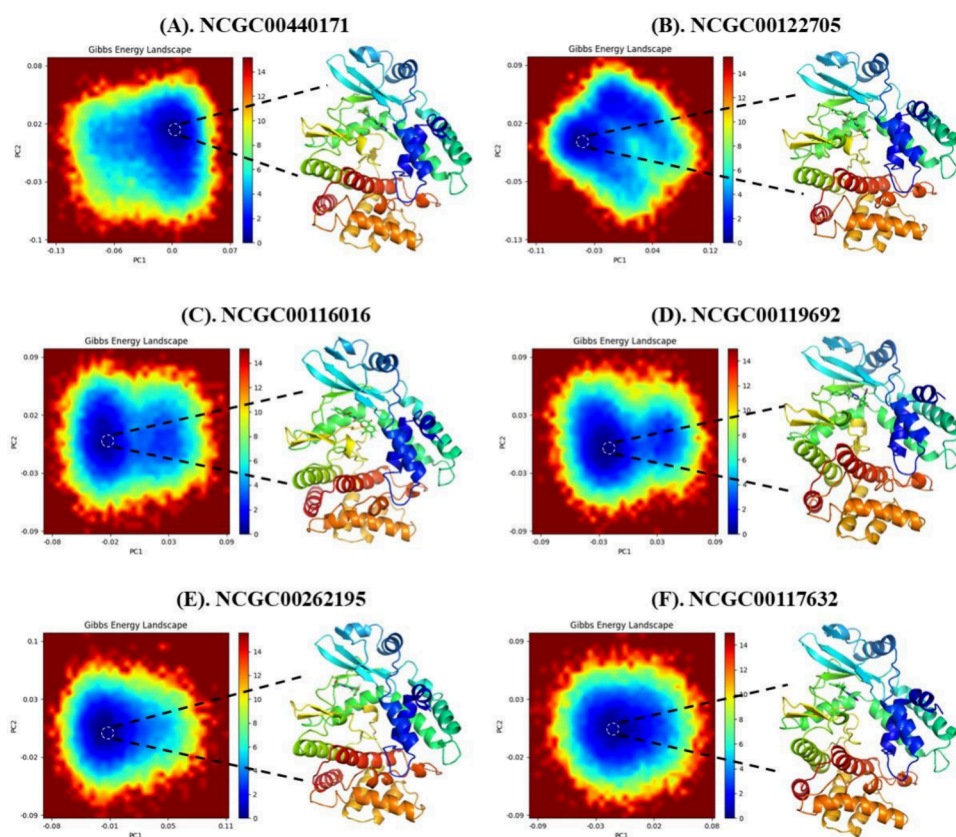 of the simulated trajectories of C α atoms within the ADCK3 protein onto the first two principal components for conformation searching was employed.

the key interactions derived from the three-point pharmacophore model. These docking hypotheses are highly consistent with the ADCK3 biochemical assay data, showing that both compounds are the most potent ones from the hit list with IC_{50} values of 0.48 and 0.34 μM, respectively. The results further demonstrate that the three-point pharmacophore captured the crucial interactions for ADCK3 inhibitors and validated the robustness of our pharmacophore-based virtual screening strategy.

In Silico Evaluation of Hits by MD Simulations with Metadynamics Analysis. In order to elucidate the binding mechanism of these identified compounds within the ADCK3 active site and provide physical chemistry insights for future studies, MD simulations were employed to describe their microinteractions within the protein active site. The physical insights provided by MD simulations could largely refine the screening results of empirical docking-based calculations. The root-mean-square fluctuation (RMSF) plots of these compounds are shown in Figure S2 of the Supporting Information. From the calculated RMSDs (Figure S3), it is evident that the simulations are well converged within 200 ns. Starting with the entire protein structure, the MD simulations accurately identified the local minimum-energy conformations, revealing the inhibitors' binding activity at the ADCK3 active site as well as the formation of stable hydrogen bonds with the surrounding residues (Figure 6). However, it is worth noting that the accuracy of these simulations in predicting the binding activities of the identified inhibitors may, to some degree, be influenced by the adequacy of the simulation time and the selected parameters, particularly in cases where steric

hindrance is present. Furthermore, the spatial selectivity of the ADCK3 protein pocket is the major contributing factor to the stable conformations of the protein−inhibitor complex systems obtained by MD simulation (indicated by the dark-blue region in Figure 6), and the conformational flexibility of the identified inhibitors is also important for their binding activity. To improve sampling, we performed in-depth metadynamics analysis. The calculated free energies for these compounds further demonstrated that they are dominantly noncovalent binders. (Free-energy calculation results are presented in Table 1.) Although the exact ranking order between the IC_{50} values determined from the ADCK3 biochemical assay and the binding free energy is not highly correlated, a clear trend is still observable: highly potent compounds (nanomolar potency, such as for NCGC00440171, NCGC00262195, and NCGC00117632) correlate with lower calculated binding free energies in MD analysis, and moderately active compounds (micromolar potency, such as for NCGC00122705 and NCGC00119692) correlate with higher calculated binding free energies. The only exception among the top-ranking hits is NCGC00116016. It is crucial to acknowledge that the accuracy of binding free-energy calculations relies heavily on the chosen method and that binding conformations can significantly influence the calculation results, potentially causing deviations from the experimental measurements. Additionally, we recognize that the inclusion of only six compounds in this study limits the robustness of our statistical analysis. From the quantitative calculation results, we also noticed that the van der Waals (vdW) and electrostatic interactions play dominant roles in the

protein−inhibitor binding (Figure S4). Through a comparative analysis with the binding free energies and experimentally observed inhibitory activities, we further noticed that these two values are highly associated with each other but not strictly positively correlated. Such a theoretical clarification provides a good starting point for medicinal chemistry optimization in future for ADCK3 structure-based drug development.

CONCLUSIONS

The virtual screening technologies can efficiently identify drug candidates for specific targets with high accuracy at an affordable cost. Therefore, this is an important complementary approach to experimental high-throughput screening. In this study, we employed a pharmacophore-based virtual screen that yielded novel compounds targeting the ATP-binding site of ADCK3, without any prior structural knowledge of small-molecule inhibitors. The pharmacophore query could enhance the speed and accuracy of large-scale docking trials through quantitative targeting specific interactions in the hinge region. This approach enabled the discovery of novel small-molecule ADCK3 inhibitors, with the top-ranking hits demonstrating nanomolar potency in the ADCK3 biochemical assay with selectivity against the p38 counter-target. The binding modes of the most potent compounds were also elucidated by MD simulations and metadynamics analysis. The key amino acid residues governing intermolecular interactions were discussed, providing guidance for further medicinal chemistry optimization to improve potency and selectivity. Although previous ADCK3 inhibitors have been reported,[16,20] this study applied a combinatorial VS strategy to rapidly identify novel chemical series of ADCK3 inhibitors without a laborious and time-consuming high-throughput screening campaign. In principle, this novel strategy can be extended to any target-based screening, and it can quickly expand the molecular diversity coverage of the potential inhibitors. Therefore, the combination methodology proposed in this study represents a promising strategy for accelerated drug discovery.

ASSOCIATED CONTENT

Data Availability Statement

The computational files and technique details can be found in our GitHub page: https://github.com/tcsnfrank0177/ADCK3Target_VirtualScreening.

Supporting Information

The Supporting Information is available free of charge at https://pubs.acs.org/doi/10.1021/acs.jcim.4c00530.

    QC data for the lead compounds (XLSX)

    Root-mean-square deviations (RMSDs) for MD simulations and binding activity analysis of the lead compounds (PDF)

AUTHOR INFORMATION

Corresponding Authors

Wei Zheng − *Therapeutics Development Branch, Division of Preclinical Innovation, National Center for Translational Sciences (NCATS), National Institutes of Health (NIH), Rockville, Maryland 20850, United States*; Email: wzheng@mail.nih.gov

Min Shen − *Early Translation Branch, Division of Preclinical Innovation, National Center for Translational Sciences (NCATS), National Institutes of Health (NIH), Rockville,*

Maryland 20850, United States; orcid.org/0000-0002-8218-0433; Email: shenmin@mail.nih.gov

Authors

Peng Gao − *Therapeutics Development Branch, Division of Preclinical Innovation, National Center for Translational Sciences (NCATS), National Institutes of Health (NIH), Rockville, Maryland 20850, United States;* orcid.org/0000-0001-5669-9007

Mitali Tambe − *Therapeutics Development Branch, Division of Preclinical Innovation, National Center for Translational Sciences (NCATS), National Institutes of Health (NIH), Rockville, Maryland 20850, United States*

Catherine Z. Chen − *Therapeutics Development Branch, Division of Preclinical Innovation, National Center for Translational Sciences (NCATS), National Institutes of Health (NIH), Rockville, Maryland 20850, United States*

Wenwei Huang − *Therapeutics Development Branch, Division of Preclinical Innovation, National Center for Translational Sciences (NCATS), National Institutes of Health (NIH), Rockville, Maryland 20850, United States;* orcid.org/0000-0002-7727-9287

Gregory J. Tawa − *Therapeutics Development Branch, Division of Preclinical Innovation, National Center for Translational Sciences (NCATS), National Institutes of Health (NIH), Rockville, Maryland 20850, United States*

Tal Hirschhorn − *Department of Biological Sciences, Department of Chemistry and Department of Pathology and Cell Biology, Columbia University, New York, New York 10027, United States*

Brent R. Stockwell − *Department of Biological Sciences, Department of Chemistry and Department of Pathology and Cell Biology, Columbia University, New York, New York 10027, United States;* orcid.org/0000-0002-3532-3868

Complete contact information is available at:
https://pubs.acs.org/10.1021/acs.jcim.4c00530

Notes

The authors declare the following competing financial interest(s): B.R.S. co-founded and serves as a consultant to ProJenX, Inc. and Exarta Therapeutics, holds equity in Sonata Therapeutics, and serves as a consultant to Weatherwax Biotechnologies Corporation and Akin Gump Strauss Hauer & Feld LLP. The remaining authors declare no competing interests.

ACKNOWLEDGMENTS

REFERENCES

(1) Stefely, J. A.; Pagliarini, D. J. Biochemistry of Mitochondrial Coenzyme Q Biosynthesis. *Trends Biochem. Sci.* **2017**, *42* (10), 824−843.

(2) Acosta, M. J.; Vazquez Fonseca, L.; Desbats, M. A.; Cerqua, C.; Zordan, R.; Trevisson, E.; Salviati, L. Coenzyme Q biosynthesis in

health and disease. *Biochimica et Biophysica Acta (BBA) - Bioenergetics* **2016**, *1857* (8), 1079−1085.

(3) Barca, E.; Musumeci, O.; Montagnese, F.; Marino, S.; Granata, F.; Nunnari, D.; Peverelli, L.; DiMauro, S.; Quinzii, C. M.; Toscano, A. Cerebellar ataxia and severe muscle CoQ10 deficiency in a patient with a novel mutation in ADCK3. *Clinical Genetics* **2016**, *90* (2), 156−160. Barca, E.; Musumeci, O.; Peverelli, L.; Ciranni, A.; DiMauro, S.; Hirano, M.; Quinzii, C. M.; Toscano, A. Cerebellar Ataxia with CoQ10 Deficiency Due to a Novel Mutation in ADCK3 (P6. 057). AAN Enterprises: 2014. Shalata, A.; Edery, M.; Habib, C.; Genizi, J.; Mahroum, M.; Khalaily, L.; Assaf, N.; Segal, I.; Abed El Rahim, H.; Shapira, H.; et al. Primary Coenzyme Q deficiency Due to Novel ADCK3 Variants, Studies in Fibroblasts and Review of Literature. *Neurochem. Res.* **2019**, *44* (10), 2372−2384.

(4) Stefely, J. A.; Licitra, F.; Laredj, L.; Reidenbach, A. G.; Kemmerer, Z. A.; Grangeray, A.; Jaeg-Ehret, T.; Minogue, C. E.; Ulbrich, A.; Hutchins, P. D. Cerebellar ataxia and coenzyme Q deficiency through loss of unorthodox kinase activity. *Molecular cell* **2016**, *63* (4), 608−620. Stefely, J. A.; Reidenbach, A. G.; Ulbrich, A.; Oruganty, K.; Floyd, B. J.; Jochem, A.; Saunders, J. M.; Johnson, I. E.; Minogue, C. E.; Wrobel, R. L. Mitochondrial ADCK3 employs an atypical protein kinase-like fold to enable coenzyme Q biosynthesis. *Molecular cell* **2015**, *57* (1), 83−94.

(5) Gräter, F.; Shen, J.; Jiang, H.; Gautel, M.; Grubmüller, H. Mechanically induced titin kinase activation studied by force-probe molecular dynamics simulations. *Biophysical journal* **2005**, *88* (2), 790−804. Frembgen-Kesner, T.; Elcock, A. H. Computational sampling of a cryptic drug binding site in a protein receptor: explicit solvent molecular dynamics and inhibitor docking to p38 MAP kinase. *Journal of molecular biology* **2006**, *359* (1), 202−214. Dago, A. E.; Schug, A.; Procaccini, A.; Hoch, J. A.; Weigt, M.; Szurmant, H. Structural basis of histidine kinase autophosphorylation deduced by integrating genomics, molecular dynamics, and mutagenesis. *Proc. Natl. Acad. Sci. U. S. A.* **2012**, *109* (26), E1733−E1742. Aci-Sèche, S.; Ziada, S.; Braka, A.; Arora, R.; Bonnet, P. Advanced molecular dynamics simulation methods for kinase drug discovery. *Future medicinal chemistry* **2016**, *8* (5), 545−566. Thirumal Kumar, D.; George Priya Doss, C. Role of E542 and E545 missense mutations of PIK3CA in breast cancer: a comparative computational approach. *J. Biomol. Struct. Dyn.* **2017**, *35* (12), 2745−2757.

(6) Vilar, S.; Cozza, G.; Moro, S. Medicinal Chemistry and the Molecular Operating Environment (MOE): Application of QSAR and Molecular Docking to Drug Discovery. *Current Topics in Medicinal Chemistry* **2008**, *8* (18), 1555−1572.

(7) Gao, P.; Xu, M.; Zhang, Q.; Chen, C. Z.; Guo, H.; Ye, Y.; Zheng, W.; Shen, M. Graph Convolutional Network-Based Screening Strategy for Rapid Identification of SARS-CoV-2 Cell-Entry Inhibitors. *J. Chem. Inf. Model.* **2022**, *62* (8), 1988−1997. Gao, P.; Zhang, Q.; Keely, D.; Cleveland, D. W.; Ye, Y.; Zheng, W.; Shen, M.; Yu, H. Molecular Graph-Based Deep Learning Algorithm Facilitates an Imaging-Based Strategy for Rapid Discovery of Small Molecules Modulating Biomolecular Condensates. *J. Med. Chem.* **2023**, *66* (22), 15084−15093.

(8) Trott, O.; Olson, A. J. AutoDock Vina: improving the speed and accuracy of docking with a new scoring function, efficient optimization, and multithreading. *Journal of computational chemistry* **2010**, *31* (2), 455−461.

(9) Forli, S.; Huey, R.; Pique, M. E.; Sanner, M. F.; Goodsell, D. S.; Olson, A. J. Computational protein−ligand docking and virtual drug screening with the AutoDock suite. *Nature protocols* **2016**, *11* (5), 905−919.

(10) Wallace, A. C.; Laskowski, R. A.; Thornton, J. M. LIGPLOT: a program to generate schematic diagrams of protein-ligand interactions. *Protein engineering, design and selection* **1995**, *8* (2), 127−134. Yuan, S.; Chan, H. S.; Hu, Z. Using PyMOL as a platform for computational drug design. *Wiley Interdisciplinary Reviews: Computational Molecular Science* **2017**, *7* (2), No. e1298.

(11) Bjelkmar, P.; Larsson, P.; Cuendet, M. A.; Hess, B.; Lindahl, E. Implementation of the CHARMM force field in GROMACS: analysis of protein stability effects from correction maps, virtual interaction sites, and water models. *J. Chem. Theory Comput.* **2010**, *6* (2), 459−466.

(12) Brooks, B. R.; Brooks, C. L., III; Mackerell, A. D., Jr; Nilsson, L.; Petrella, R. J.; Roux, B.; Won, Y.; Archontis, G.; Bartels, C.; Boresch, S. CHARMM: the biomolecular simulation program. *Journal of computational chemistry* **2009**, *30* (10), 1545−1614. Jo, S.; Kim, T.; Iyer, V. G.; Im, W. CHARMM-GUI: a web-based graphical user interface for CHARMM. *Journal of computational chemistry* **2008**, *29* (11), 1859−1865. Lee, J.; Cheng, X.; Jo, S.; MacKerell, A. D.; Klauda, J. B.; Im, W. CHARMM-GUI input generator for NAMD, GROMACS, AMBER, OpenMM, and CHARMM/OpenMM simulations using the CHARMM36 additive force field. *Biophysical journal* **2016**, *110* (3), 641a. Lou, H.; Cukier, R. I. Molecular dynamics of apo-adenylate kinase: a principal component analysis. *J. Phys. Chem. B* **2006**, *110* (25), 12796−12808.

(13) Mark, P.; Nilsson, L. Structure and dynamics of the TIP3P, SPC, and SPC/E water models at 298 K. *J. Phys. Chem. A* **2001**, *105* (43), 9954−9960.

(14) Bussi, G.; Donadio, D.; Parrinello, M. Canonical sampling through velocity rescaling. *J. Chem. Phys.* **2007**, *126* (1), 014101.

(15) Berendsen, H. J.; Postma, J. v.; Van Gunsteren, W. F.; DiNola, A.; Haak, J. R. Molecular dynamics with coupling to an external bath. *J. Chem. Phys.* **1984**, *81* (8), 3684−3690.

(16) Asquith, C. R.; Berger, B.-T.; Wan, J.; Bennett, J. M.; Capuzzi, S. J.; Crona, D. J.; Drewry, D. H.; East, M. P.; Elkins, J. M.; Fedorov, O. SGC-GAK-1: a chemical probe for cyclin G associated kinase (GAK). *Journal of medicinal chemistry* **2019**, *62* (5), 2830−2836.

(17) Chantarasakha, K.; Asawapanumas, T.; Suntivich, R.; Panya, A.; Phonsatta, N.; Thiennimitr, P.; Laoteng, K.; Tepaamorndech, S. Hatakabb, a herbal extract, contains pyrogallol as the novel mediator inhibiting LPS-induced TNF-α production by NF-κB inactivation and HMOX-1 upregulation. *Journal of Functional Foods* **2022**, *90*, 104992.

(18) Inglese, J.; Auld, D. S.; Jadhav, A.; Johnson, R. L.; Simeonov, A.; Yasgar, A.; Zheng, W.; Austin, C. P. Quantitative high-throughput screening: A titration-based approach that efficiently identifies biological activities in large chemical libraries. *Proc. Natl. Acad. Sci. U. S. A.* **2006**, *103* (31), 11473−11478.

(19) Goldstein, D. M.; Soth, M.; Gabriel, T.; Dewdney, N.; Kuglstatter, A.; Arzeno, H.; Chen, J.; Bingenheimer, W.; Dalrymple, S. A.; Dunn, J. Discovery of 6-(2, 4-Difluorophenoxy)-2-[3-hydroxy-1-(2-hydroxyethyl) propylamino]-8-methyl-8 H-pyrido [2, 3-d] pyrimidin-7-one (Pamapimod) and 6-(2, 4-Difluorophenoxy)-8-methyl-2-(tetrahydro-2 H-pyran-4-ylamino) pyrido [2, 3-d] pyrimidin-7 (8 H)-one (R1487) as Orally Bioavailable and Highly Selective Inhibitors of p38α Mitogen-Activated Protein Kinase. *J. Med. Chem.* **2011**, *54* (7), 2255−2265.

(20) Murray, N. H.; Asquith, C. R.; Fang, Z.; East, M. P.; Ptak, N.; Smith, R. W.; Vasta, J. D.; Zimprich, C. A.; Corona, C. R.; Robers, M. B. Small-molecule inhibition of the archetypal UbiB protein COQ8. *Nat. Chem. Biol.* **2023**, *19* (2), 230−238.